



Texture of Nanocrystalline Nickel: Probing the Lower Size Limit of Dislocation Activity

Bin Chen *et al.*

Science **338**, 1448 (2012);

DOI: 10.1126/science.1228211

This copy is for your personal, non-commercial use only.

If you wish to distribute this article to others, you can order high-quality copies for your colleagues, clients, or customers by [clicking here](#).

Permission to republish or repurpose articles or portions of articles can be obtained by following the guidelines [here](#).

The following resources related to this article are available online at www.sciencemag.org (this information is current as of December 14, 2012):

Updated information and services, including high-resolution figures, can be found in the online version of this article at:

<http://www.sciencemag.org/content/338/6113/1448.full.html>

Supporting Online Material can be found at:

<http://www.sciencemag.org/content/suppl/2012/12/12/338.6113.1448.DC1.html>

This article **cites 32 articles**, 9 of which can be accessed free:

<http://www.sciencemag.org/content/338/6113/1448.full.html#ref-list-1>

This article appears in the following **subject collections**:

Materials Science

http://www.sciencemag.org/cgi/collection/mat_sci

32. D. N. Burrows *et al.*, *Nature* **476**, 421 (2011).
 33. S. B. Cenko *et al.*, *Astrophys. J.* **753**, 77 (2012).
 34. J. S. Bloom *et al.*, *Science* **333**, 203 (2011).
 35. M. G. Akritas, M. A. Bershad, *Astrophys. J.* **470**, 706 (1996).
 36. To include the tidal disruption flares in Fig. 1, we used the Fermi LAT upper limit (32) observed for Swift J164449.3+573451, and we assumed $L^{\text{iso}} \sim L_x$ for Swift J2058.4+0516 (33), where L_x is the observed x-ray luminosity. We assumed $P_{\text{jet}} \sim L_{\text{Edd}}$, where L_{Edd} is the Eddington luminosity based on the black hole masses estimated in (32–34). These luminosities and powers should be treated as upper limits.

Acknowledgments: We thank J. Racusin, M. Lister, C. Dermer, A. Pushkarev, J. McEnery, D. Donato, D. Kazanas, T. Nelson, and F. Tombesi for crucial discussions. R.S.N. and S.G. were supported by an appointment to the NASA Postdoctoral Program at Goddard Space Flight Center, administered by Oak Ridge Associated Universities through a contract with NASA. This research has made use of: (i) StatCodes statistical software hosted by The Pennsylvania State University's Center for Astrostatistics; (ii) data obtained from the HETE science team via the Web site <http://space.mit.edu/HETE/Bursts/Data> (HETE is an international mission of the NASA Explorer program, run by the Massachusetts Institute of Technology); and (iii) NASA/IPAC Extragalactic Database (NED), which is

operated by the Jet Propulsion Laboratory, California Institute of Technology, under contract with NASA.

Supplementary Materials

www.sciencemag.org/cgi/content/full/338/6113/1445/DC1
 Supplementary Text
 Fig. S1
 Tables S1 to S4
 References (37–75)

13 July 2012; accepted 1 November 2012
 10.1126/science.1227416

Texture of Nanocrystalline Nickel: Probing the Lower Size Limit of Dislocation Activity

Bin Chen,^{1,2*} Katie Lutker,³ Selva Vennila Raju,^{1,2,4} Jinyuan Yan,^{1,2} Waruntorn Kanitpanyacharoen,⁵ Jialin Lei,⁶ Shizhong Yang,⁶ Hans-Rudolf Wenk,⁵ Ho-kwang Mao,^{7,8} Quentin Williams²

The size of nanocrystals provides a limitation on dislocation activity and associated stress-induced deformation. Dislocation-mediated plastic deformation is expected to become inactive below a critical particle size, which has been proposed to be between 10 and 30 nanometers according to computer simulations and transmission electron microscopy analysis. However, deformation experiments at high pressure on polycrystalline nickel suggest that dislocation activity is still operative in 3-nanometer crystals. Substantial texturing is observed at pressures above 3.0 gigapascals for 500-nanometer nickel and at greater than 11.0 gigapascals for 20-nanometer nickel. Surprisingly, texturing is also seen in 3-nanometer nickel when compressed above 18.5 gigapascals. The observations of pressure-promoted texturing indicate that under high external pressures, dislocation activity can be extended down to a few-nanometers-length scale.

The plastic behavior of coarse-grained metals (with particle size >100 nm) is mainly controlled by the nucleation and motion of lattice dislocations. Plastic deformation by dislocation glide results in crystallite rotations, generating lattice-preferred orientation or texture. The anisotropic physical properties of a polycrystalline material are strongly related to the preferred alignment of its crystallites. In material science and engineering, texture control is essential in improving the strength and lifetime of structural materials (1). In Earth science, understanding texture development of minerals is important for interpreting seismic anisotropy in Earth's interior (2).

How plastic deformation occurs in nanocrystalline materials remains controversial (3–5).

¹Advanced Light Source, Lawrence Berkeley National Lab, Berkeley, CA 94720, USA. ²Department of Earth and Planetary Sciences, University of California, Santa Cruz, Santa Cruz, CA 95064, USA. ³Department of Chemistry, University of California, Berkeley, Berkeley, CA 94720, USA. ⁴Department of Physics, University of Nevada, Las Vegas, NV 89119, USA. ⁵Department of Earth and Planetary Science, University of California, Berkeley, Berkeley, CA 94720, USA. ⁶Louisiana Optical Network Initiative (LONI) Institute, Southern University, Baton Rouge, LA 70813, USA. ⁷Geophysical Laboratory, Carnegie Institution of Washington, Washington, DC 20015, USA. ⁸Center for High Pressure Science and Technology Advanced Research, Shanghai 201203, China.

*To whom correspondence should be addressed. E-mail: bchen@lbl.gov

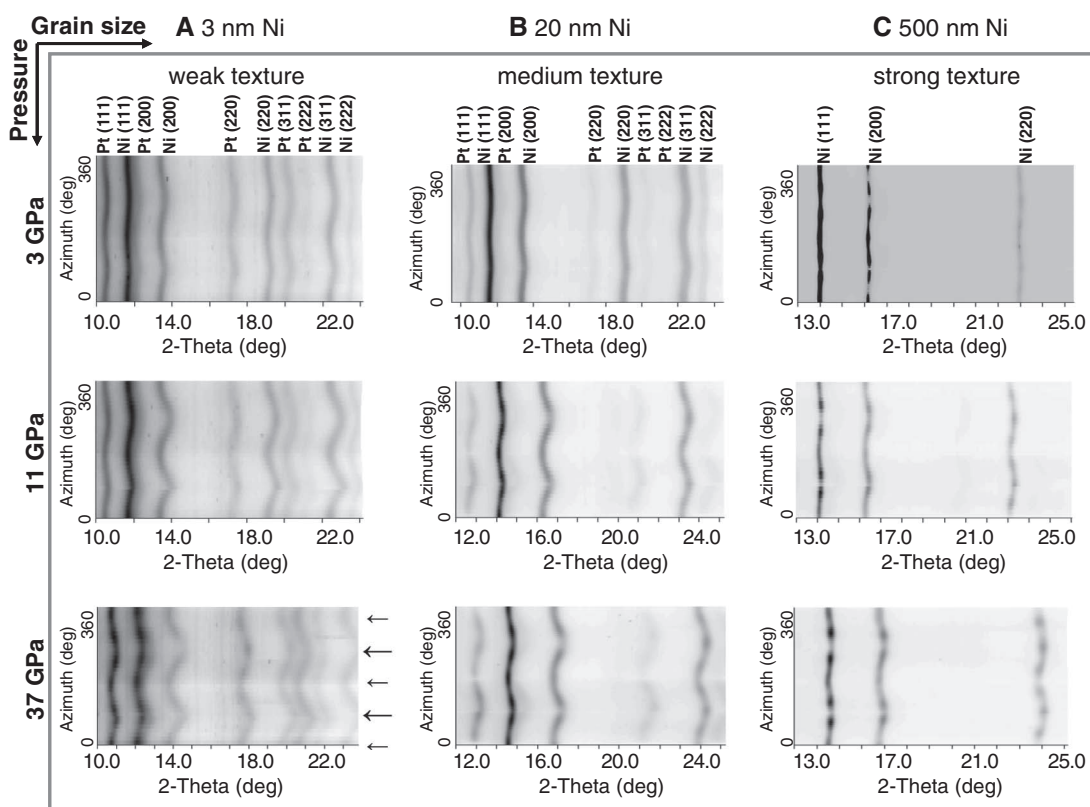
Post-deformation analysis of compressed or indented nanocrystalline nickel does not indicate major dislocation debris (12), whereas dislocations are observed in 10-nm nickel and 9-nm platinum particles (13, 14). Deformation twinning and disclination have also been reported in several studies on nanocrystals (6, 9–11, 15). Although it is commonly believed that the intrinsic deformation behavior of nanomaterials arise from the interplay between defects and grain-boundary (GB) processes (11, 16), the precise trade-offs between these deformation mechanisms are still unclear, as is the effect of pressure on these different mechanisms. It has been proposed that below a critical length scale, the strength of nanometals would exhibit an inverse Hall-Petch size dependence because in the plastic deformation of fine nanocrystals, dislocation activity gives way to GB sliding, diffusion, and grain rotation (4, 5). In contrast, twin thickness has been found to affect the maximum strength of copper, implying that the plastic deformation of nanomaterials is not necessarily related to GB-mediated processes (9). Indeed, it has been proposed that dislocation nucleation governs material softening in nano-twinned metals (10).

Because of technical limitations, in situ observation of plastic deformation in ultrafine nanocrystals is difficult, precluding the direct exploration of mechanics at nanometer scales. Whether plas-

ticity in ultrafine nanocrystals is still generated by dislocations, how pressure affects the deformational regimes of nanoparticles, and how structural anisotropy is affected by size reductions are all unresolved questions. The effect of pressure on dislocations is complex in terms of both the high-pressure energetics of dislocation cores and their mobilities, with the net overarching effects of pressure being unclear (17). It has been observed that at high pressure, brittle materials such as oxides and silicates become ductile, even at room temperature (2). Our goal is to examine the interplay between pressure and particle size in determining when dislocation-mediated deformation processes predominate within nanoparticles and, correspondingly, what the lower size limit of dislocation activity is. In this work, radial diamond anvil cell (rDAC) x-ray diffraction (XRD) experiments (2) were used to make in situ observation of the texturing in stressed polycrystalline nickel of various mean particle sizes, from 500 nm down to 3 nm.

We deformed the nickel samples plastically in rDACs (fig. S1) (18). The XRD experiments were performed at beamline 12.2.2, Advanced Light Source (ALS), Lawrence Berkeley National Laboratory. The particle sizes of the nickel samples are 500 ± 45 nm, 20 ± 8 nm, and 3 ± 0.9 nm (fig. S2) (18), respectively. The relatively narrow size distributions allow the investigation of the size dependence of texturing. When shear stress is applied to polycrystals, individual crystals deform preferentially on slip planes. This results in crystal rotations that in turn lead to texture development (1). The radial diffraction images show variations in diffraction peak position with respect to the compression direction, indicating differential stresses in the material. They also display systematic intensity variations that can be used to deduce texture (Fig. 1 and figs. S3 to S6) (18). For instance, the diffraction intensity of the 500-nm nickel at 5.0 GPa is minimal in the compression direction for the (200) diffraction peak but maximal for the (220) peak (fig. S3). Diffraction intensity variations are seen in the 500-nm nickel above 3.0 GPa and in 20-nm nickel above 11.0 GPa, and more modest but resolvable intensity variations are observed in 3-nm nickel at pressures above 18.5 GPa. The variations in diffraction intensity can be best seen in the “unrolled diffraction” images recorded as a function of diffraction angle (Fig. 1).

Fig. 1. Azimuthally (0 to 360°) unrolled diffraction images of (A) 3-nm, (B) 20-nm, and (C) 500-nm nickel. To enable direct comparison between runs, pressures are rounded (precise values are given in Fig. 2). The long thick arrows indicate the maximum compression direction, and the short thin arrows indicate the minimum compression direction. The curvature within the diffraction lines indicates that the sample is stressed. Texture is evident as the systematic intensity variations of the diffraction peaks along the azimuthal direction. Some images contain mixed diffraction from the nickel sample and the platinum pressure calibrant. The diffraction of 20-nm particles at 3 GPa and 3-nm particles at 37 GPa was taken with an x-ray wavelength of 0.4133 Å. For all other measurements, a wavelength of 0.4959 Å was used.



Rietveld refinement, implemented in the MAUD software (19), was used to analyze the differential stress, microstructure, and texture of the samples at each pressure. Texture is represented with inverse pole figures of the compression direction (Fig. 2 and fig. S7): These show the probability of finding the poles (normal) to lattice planes in the compression direction. The texture in the 500-nm nickel evolves at pressures as low as 3.0 GPa (Fig. 2 and fig. S8). Texture strength—the degree of lattice-preferred orientation (18)—increases to 2.4 multiples of random distribution (MRD) at 35.0 GPa. In the experiment with the 20-nm nickel, obvious texture starts to develop at 11.0 GPa with 1.7 MRD. Upon further compression to 38.5 GPa, the texture strength of the 20-nm nickel increases to 2.0 MRD. In the 3-nm nickel experiment, a weak but substantial texture (1.4 MRD) is observed upon compression above 18 GPa. The texture observations indicate that dislocation-mediated plastic deformation is still active in the 3-nm nickel when high external pressure is applied. It is known that dislocation glide on preferred slip systems gives rise to crystallographic texture, whereas grain rotation via GB sliding alone randomizes the grain orientation distribution (3). The GB activities are believed to be more active in smaller nanocrystals. The observed decrease of texture strength with decreasing particle size indicates that the texturing is not primarily derived from GB processes. Our separate measurements show that carbon-coated nickel nanocrystals, when deformed at high pressure, have similar texturing to pure

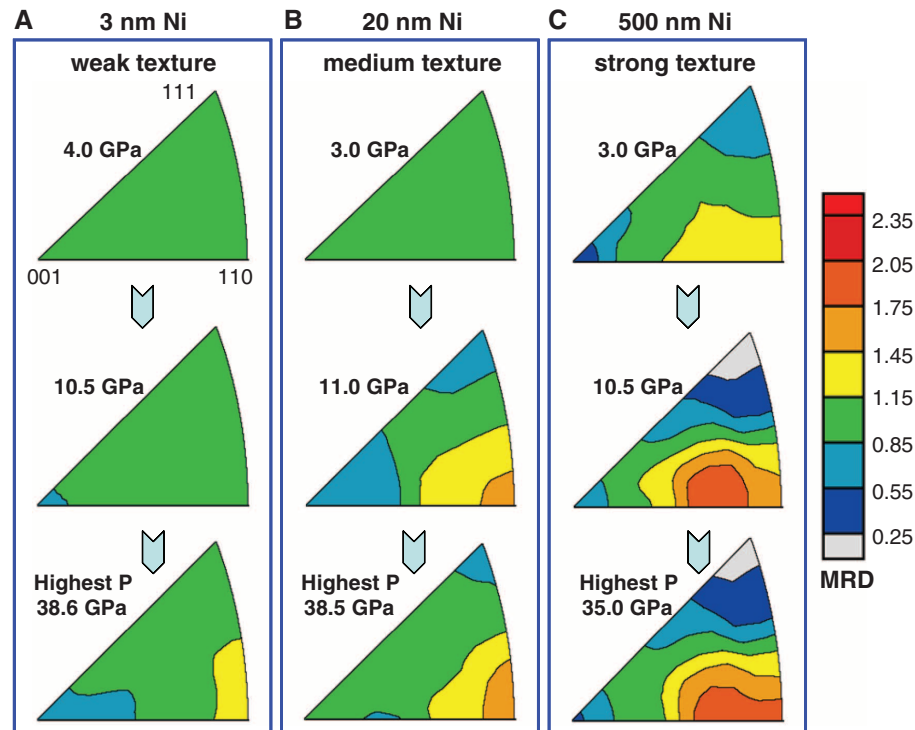


Fig. 2. Inverse pole figures of (A) 3-nm, (B) 20-nm, and (C) 500-nm nickel along the compression direction (normal direction). Equal area projection and a linear scale are used. Texture strength is expressed as MRD, where MRD = 1 denotes random distribution, and a higher MRD number represents stronger texture.

nickel particles of the same size (fig. S9), which strongly supports that the observed texturing is not arising from GB processes.

As shown in Fig. 1, at the same pressures the differential strain of the 3-nm nickel is higher than that of coarser particles. The larger curvatures

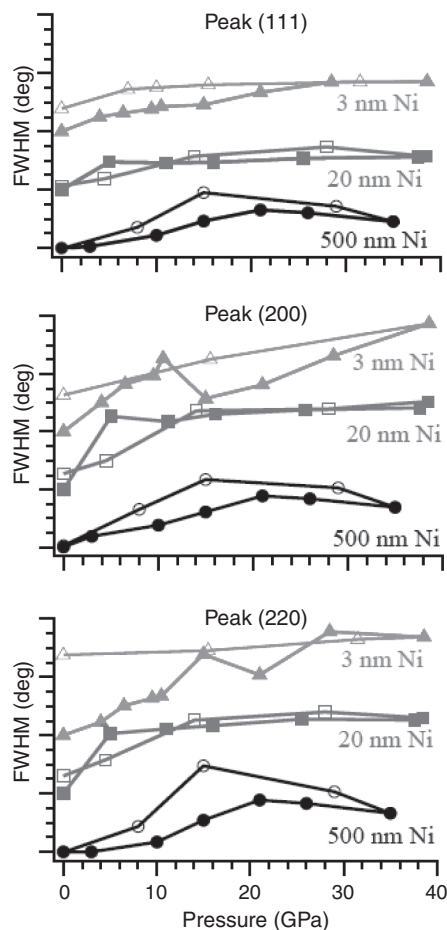


Fig. 3. The peak broadening of the nickel in compression relative to ambient pressure. The full width at half maximum (FWHM) is determined in terms of diffraction angle, 2θ . The curves are offset for clarity, and the small ticks represent 0.05° . For the FWHM determination, the signal is integrated over 10° around the compression direction. The solid symbols represent compression data, whereas the open symbols are decompression data. The lines connecting the data points are guides for the eye.

of diffraction lines for smaller particles indicate higher elastic deformation and greater ability for the material to support the differential stress in the crystal plane without plastic deformation (20). From the lattice strain, shear stress can be estimated (18). According to the MAUD analysis, the differential stress on the 3-nm nickel is 8.0 GPa at an external pressure of 38.6 GPa, for the 20-nm nickel is 5.1 GPa at 38.5 GPa external pressure, and for 500-nm nickel is 2.9 GPa at 35.0 GPa external pressure. Differences in the level of dislocation activity are likely to account for these systematic variations. Lower dislocation contents and reduced mobility due to the enhanced dislocation-GB interaction in smaller particles could result in pinned dislocations, so elastic stress, built up in compression, is only minimally released by plastic deformation.

To obtain additional insights into the plastic deformation process, we studied the x-ray peak

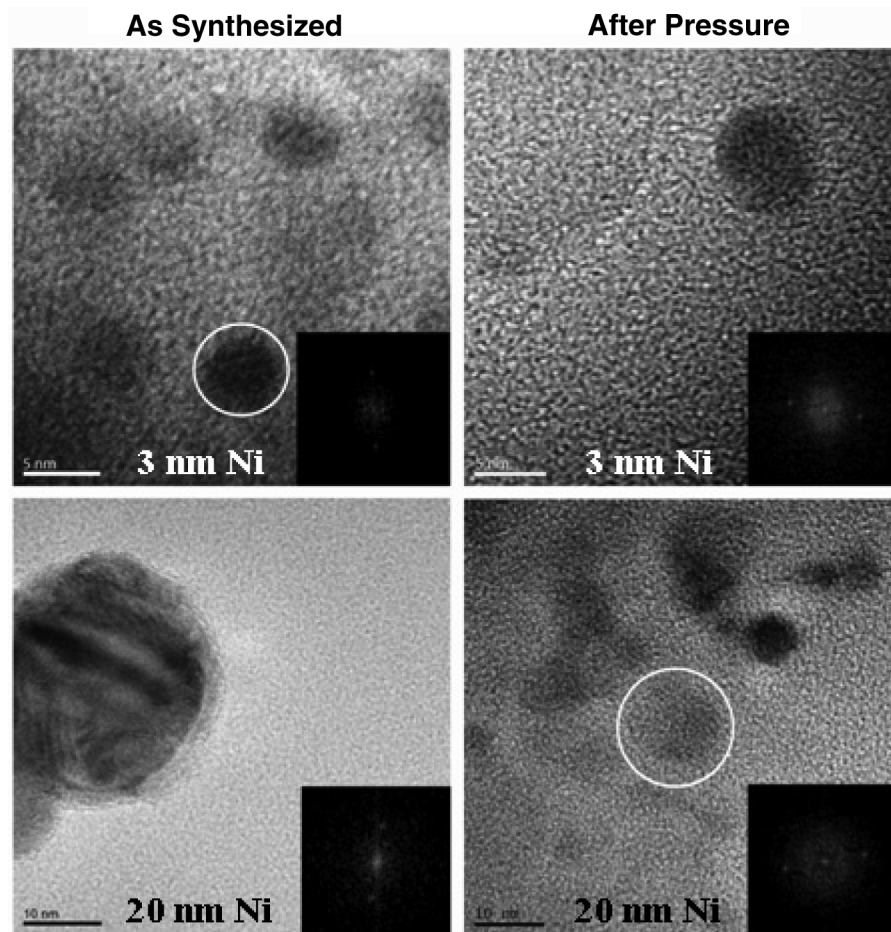


Fig. 4. Representative high-resolution TEM images of the (top) 3- and (bottom) 20-nm nickel particles as synthesized and as recovered from compression. The insets show the Fourier transforms of the particle images, indicating the absence of lattice defects before and after pressure. When more than one particle is present in the image, the inset corresponds to the circled particle. In the image of the 20-nm nickel particles after compression, only the circled particle was isolated; the other particles were not isolated and were damaged under the electron beam.

broadening of the samples at high pressures (Fig. 3). It is known that peak broadening is generated by several factors, including instrumental broadening, grain size effects, and stress (microstrain)-induced broadening (21). A standard material, LaB_6 , was used to characterize the instrumental broadening. The peak broadening of unstressed samples was used to confirm the particle size that was measured with transmission electron microscopy (TEM) and scanning EM (Fig. 4 and fig. S2). It has been verified that there is usually no particle coarsening and associated peak width reduction under compression if there are no crystallite domain changes, as are produced by phase transformations (22). Thus, it is reasonable to ascribe the observed peak broadening to local stresses produced by inhomogeneous strain (9).

The evolution of peak broadening of the three stressed samples shows substantial differences (Fig. 3). The broadenings of the three peaks of the coarse particles have similar pressure dependencies, whereas the broadenings of the three peaks of 3-nm nickel evolve differently with pressure. This difference likely arises from varying

sensitivities of the differently sized particles to particle shape change. Pressure-induced particle shape changes in fine nanocrystals could result in peak width changes (23). Strain profiles in compression also affect peak broadening. In the 500-nm nickel, the peak broadening increases to a maximum as pressure is increased to ~ 21.0 GPa, indicating that peak broadening in this pressure range mainly comes from the elastic strain. Upon further compression, the peak broadening decreases slightly. Although the observation of texture in 500-nm nickel indicates the existence of dislocations above 3.0 GPa, the increased plastic strain does not dominate the local strain up to a pressure of 21.0 GPa. In the 20-nm nickel, there is not much enhancement of peak broadening in compression above ~ 5 GPa, indicating that plastic strain dominates the peak broadening, which suggests that other mechanisms probably dominate the plastic deformation before the onset of texturing. The peak broadening in the 3-nm particles is substantially less reversible on decompression than those of the two coarser samples (Fig. 3). The straightness

Table 1. Calculated critical shear stress needed for nucleation of dislocations (Eqs. 1 and 2) and the measured shear stress at the onset of texturing in nickel. For the calculations, $b_f = 0.487$ nm, $b_p = 0.244$ nm (7), $G = 76$ GPa (24, 26), $\gamma = 120$ to 130 mJ/m² (27), and $\nu = 0.31$ (26).

Type of dislocations	Particle size of nickel					
	3 nm		20 nm		500 nm	
	Edge (GPa)	Screw (GPa)	Edge (GPa)	Screw (GPa)	Edge (GPa)	Screw (GPa)
Critical shear stress for nucleation of a full dislocation (theoretical)	12.3 (2.8*)	37.0	1.8	5.4	0.1	0.2
Critical shear stress for nucleation of a partial dislocation (theoretical)	6.7	19.1	1.4	3.3	0.5	0.6
Shear stress at the onset of texturing (this experiment)	2.4		1.7		0.2	

*When dislocation-GB interactions are considered.

of the unrolled diffraction lines of the quenched sample indicates that the residual stress is negligible. GB-mediated plastic deformation does not change the crystalline domain size in the interior of the particles. Thus, the irreversibility of peak broadening in the 3-nm nickel likely originates from pressure-induced particle shape change: A modest change in shape is consistent with our TEM images (fig. S10). For comparison, the crystallographic dimension change of coarser particles due to particle shape changes may be small relative to their particle size and thus may not much affect their peak width.

Nonhydrostatic compression provides the shear stress that generates dislocation nucleation. Although the textures formed at high pressure are quenchable (figs. S3 to S5), dislocations usually cannot remain in nanocrystals when no external shear stress sustains them, which is confirmed with TEM observations (Fig. 4). The TEM measurements indicate that the nickel nanoparticles remain largely defectless single crystals after high-pressure compression. Most nickel nanoparticles after compression do appear less spherical than do precompression particles (fig. S10), and this likely arises from the nonhydrostatic pressure-induced particle shape change.

The physics governing the observed pressure-promoted texturing in nanocrystals can be understood by considering the effect of pressure on dislocations. According to dislocation theory (6, 24), with the approximation that the source size is equal to the particle size (D), the critical shear stress needed to nucleate a full dislocation is

$$\tau_f = \frac{2aGb_f}{D} \quad (1)$$

and that needed to nucleate a partial dislocation is

$$\tau_p = \frac{2aGb_p}{D} + \frac{\gamma}{b_p} \quad (2)$$

where b_f and b_p are the Burgers vectors of the full and partial dislocations, respectively; G is the shear modulus; and γ is the stacking fault energy. The factor a is taken to be 0.5 for edge dislocations and 1.5 for screw dislocations. As shown in Table 1, the critical shear stress for dislocation nucleation increases dramatically with

decreasing particle size. The measured shear stress of 500- and 20-nm nickel at the onset of texturing is quite close to the theoretically predicted values from Eqs. 1 and 2, whereas the values are discrepant for the 3-nm particles. This discrepancy is probably because the interaction of dislocations with grain boundaries is not considered in this theoretical model (6). Shan *et al.* used this model to estimate that the critical size (d_c) for nickel ranges from ~11 to 22 nm (7). The observed texturing in the 3-nm nickel suggests that under pressure, the critical size for the deformation mechanism crossover shifts to substantially smaller sizes. In small nanocrystals, dislocations are emitted and absorbed mainly at grain boundaries, and dislocation-GB interaction is highly significant for the smallest grain sizes. A simple estimation (25) of the interaction of an edge dislocation with grain boundaries can be produced from $\tau_f = \frac{Gb_f}{4\pi(1-\nu)l_{ds}}$, where ν is the Poisson's ratio and l_{ds} is the equilibrium separation between a dislocation and a grain boundary. This yields a shear stress of ~2.8 GPa for keeping an edge dislocation at the center of 3-nm nickel particles, which is in very good agreement with our measured shear stress at the onset of texturing in the 3-nm particles (Table 1). Thus, the strength of the smallest nanoparticles appears to be critically dependent on dislocation-GB interactions.

These results emphasize the importance of rDAC XRD experimentation in assessing plastic deformation in nanomaterials. Through a combination of textural and line-broadening analysis, the changing contribution of dislocation-associated deformation mechanisms can be assessed as a function of both pressure and sample particle size. Our results demonstrate that dislocation-mediated deformation persists to smaller particle sizes than anticipated. Such in situ high-pressure textural studies thus provide the means to investigate deformation mechanisms and help constrain the fundamental physics of deformation at the nanoscale.

References and Notes

1. U. F. Kocks, C. N. Tomé, H.-R. Wenk, in *Texture and Anisotropy, Preferred Orientations in Polycrystals and Their Effect on Materials Properties*, A. J. Beaudoin *et al.*, Eds. (Cambridge Univ. Press, Cambridge, ed. 2, 2000), pp. 10–531.

2. L. Miyagi, W. Kanitpanyacharoen, P. Kaercher, K. K. M. Lee, H.-R. Wenk, *Science* **329**, 1639 (2010).
 3. J. Weissmüller, J. Markmann, *Adv. Eng. Mater.* **7**, 202 (2005).
 4. J. Schiøtz, F. D. Di Tolla, K. W. Jacobsen, *Nature* **391**, 561 (1998).
 5. J. Schiøtz, K. W. Jacobsen, *Science* **301**, 1357 (2003).
 6. M. W. Chen *et al.*, *Science* **300**, 1275 (2003).
 7. Z. Shan *et al.*, *Science* **305**, 654 (2004).
 8. Z. Budrovic, H. Van Swygenhoven, P. M. Derlet, S. Van Petegem, B. Schmitt, *Science* **304**, 273 (2004).
 9. L. Lu, X. Chen, X. Huang, K. Lu, *Science* **323**, 607 (2009).
 10. X. Li, Y. Wei, L. Lu, K. Lu, H. Gao, *Nature* **464**, 877 (2010).
 11. V. Yamakov, D. Wolf, S. R. Phillpot, A. K. Mukherjee, H. Gleiter, *Nat. Mater.* **1**, 45 (2002).
 12. K. S. Kumar, S. Suresh, M. F. Chisholm, J. A. Horton, P. Wang, *Acta Mater.* **51**, 387 (2003).
 13. Z. W. Shan *et al.*, *Phys. Rev. Lett.* **98**, 095502 (2007).
 14. L. Wang *et al.*, *Phys. Rev. Lett.* **105**, 135501 (2010).
 15. M. Murayama, J. M. Howe, H. Hidaka, S. Takaki, *Science* **295**, 2433 (2002).
 16. R. L. Penn, J. F. Banfield, *Science* **281**, 969 (1998).
 17. L. Pizzagalli, J.-L. Demeenet, J. Rabier, *Phys. Rev. B* **79**, 045203 (2009).
 18. Materials and methods are available as supplementary materials on Science Online.
 19. L. Lutterotti, S. Matthies, H. Wenk, A. S. Schultz, J. W. Richardson, *J. Appl. Phys.* **81**, 594 (1997).
 20. H.-Y. Chung *et al.*, *Science* **316**, 436 (2007).
 21. I. Groma, A. Borbély, in *Diffraction Analysis of the Microstructure of Materials*, E. J. Mittemeijer, P. Scardi, Eds. (Springer-Verlag, Berlin Heidelberg, 2004), pp. 287–306.
 22. S. B. Qadri *et al.*, *J. Appl. Phys.* **89**, 115 (2001).
 23. J. N. Wickham, A. B. Herhold, A. P. Alivisatos, *Phys. Rev. Lett.* **84**, 923 (2000).
 24. T. Çağın *et al.*, *Phys. Rev. B* **39**, 12484 (1989).
 25. J. P. Hirth, J. Lothe, *Theory of Dislocations* (Krieger Publishing, Malabar, UK, ed. 2, 1992).
 26. K. Honda, Y. Shirakawa, *J. Inst. Metals. Japan* **1**, 217 (1937).
 27. C. B. Carter, S. M. Holmes, *Philos. Mag.* **35**, 1161 (1977).

Acknowledgments: B.C. and K.L. thank A. P. Alivisatos for discussions. The authors thank J. Knight, A. MacDowell, S. Clark, and A. Gleason for technical help. Financial support for this work was provided by NSF, including from the Consortium for Materials Properties Research in Earth Sciences (COMPRES) under NSF Cooperative Agreement EAR 10-43050. ALS is supported by the Director, Office of Science, Office of Basic Energy Sciences, of the U.S. Department of Energy (DOE) under contract DE-AC02-05CH11231. J.L. and S.Y. are supported by NSF-Louisiana Alliance for Simulation-Guided Materials Applications (LA-SiGMA) program (#EPS-1003897), NASA/Louisiana Education Quality Support Fund (LEQSF) (2009-2012)-Phase3-03; DOE awards DE-FE0007220, DE-FE0003693, DE-FE0004734; and the Department of Computer Science. K.L. is supported by the Physical Chemistry of Semiconductor Nanocrystals Program, KC3105, Office of Basic Energy Science of the DOE under contract DE-AC02-05CH11231. W.K. and H.R.W. thank the Carnegie/Department of Energy Alliance Center (CDAC) and the National Science Foundation (EAR-0836402) for financial support. H.-k.M. was supported as part of Energy Frontier Research in Extreme Environments Center (EFREE), an Energy Frontier Research Center funded by the DOE Office of Science, Office of Basic Energy Sciences under award DE-SG0001057. The authors thank the anonymous reviewers and M. Lavine for their helpful comments and suggestions.

Supplementary Materials

www.sciencemag.org/cgi/content/full/338/6113/1448/DC1
 Materials and Methods
 Supplementary Text
 Figs. S1 to S10
 References (28–39)

31 July 2012; accepted 19 October 2012
 10.1126/science.1228211